The fusion of early endosomes induces molecular-motor-driven tubule formation and fission

Frode M. Skjeldal[1], Sten Strunze[1], Trygve Bergeland[1], Even Walseng[1], Tone F. Gregers[1] and Oddmund Bakke[1,2,*]

[1]Centre of Immune Regulation, Department of Molecular Biosciences, University of Oslo, PB 1041 Blindern, 0316 Oslo, Norway
[2]Gades Institute, University of Bergen, The Laboratory Building, 5th floor Haukeland University Hospital, N-5021 Bergen, Norway
*Author for correspondence: (oddmund.bakke@imbv.uio.no)

Accepted 12 December 2011
Journal of Cell Science 125, 1910–1919

doi: 10.1242/jcs.092569

Summary

Organelles in the endocytic pathway interact and communicate through the crucial mechanisms of fusion and fission. However, any specific link between fusion and fission has not yet been determined. To study the endosomal interactions with high spatial and temporal resolution, we enlarged the endosomes by two mechanistically different methods: by expression of the MHC-class-II-associated chaperone invariant chain (Ii; or CD74) or Rab5, both of which increased the fusion rate of early endosomes and resulted in enlarged endosomes. Fast homotypic fusions were studied, and immediately after the fusion a highly active and specific tubule formation and fission was observed. These explosive tubule formations following fusion seemed to be a direct effect of fusion. The tubule formations were dependent on microtubule interactions, and specifically controlled by Kif16b and dynein. Our results show that fusion of endosomes is a rapid process that destabilizes the membrane and instantly induces molecular-motor-driven tubule formation and fission.

Key words: Early endosomal fusion and fission, Early endsomal tubule formation, Molecular motors

Introduction

In the endomembrane system there is a continuous remodeling of membranes through fusion and fission. Through these processes membrane dynamics are specifically controlled to maintain the membrane equilibrium and integrity from early to late endocytic compartments. The early endosome is a particularly dynamic compartment with a high fusion capacity (Gruenberg et al., 1989). Early endosomes fuse with clathrin-coated-derived vesicles and also with each other, modify their geometry through tubulation and membrane fission, move over long distances and transfer cargo to other organelles (Clague, 1998). Early endosomal homotypic fusion is a way of ensuring directionality of endocytic membrane trafficking between transport vesicles and the target organelle.

In addition to being a highly fusogenic organelle the early endosome also demonstrates a complex pleiomorphic organization of cisternal and tubular regions, membrane invaginations and multivesicularity. For the early endosome to exhibit this pleiomorphic distinctiveness, selective changes must occur in the curvature and organization of the bilayer during invagination or tubule formation (Mukherjee and Maxfield, 2000). Both extrinsic and intrinsic forces within the membrane drive the formation of tubules. Cytoskeletal elements have long been known to play some role in membrane traffic, not only by forming the structural scaffold and network controlling the vesicle trafficking, but also by directly deforming membranes (Lippincott-Schwartz et al., 2000; Vale and Hotani, 1988). Microtubule motors can pull a developing membrane tubule along a preformed microtubule track in vitro (Roux et al., 2002). Other cytoskeletal elements, such as actin filaments and membrane-tethered myosin motors, could similarly participate in membrane deformation (Buss et al., 2001; Morris et al., 2002). Additionally cytosolic proteins can alter the curvature of the lipid bilayer and participate in tubular formation (Peter et al., 2004).

To facilitate the visualization and analysis of endosomal interactions we enlarged the early endosomes by two well-described different approaches that increase fusion of early endosomes. This was done by high-level expression of either the major histocompatibility complex class II-associated invariant chain (Ii; also known as HLA class II histocompatibility antigen gamma chain or CD74) (Nordeng et al., 2002; Stang and Bakke, 1997) or Rab5 (Roberts et al., 1999). We observed an explosive tubular formation and fission immediately after the fusion, a process specifically controlled by microtubule motors.

Results

Rapid fusion of enlarged early endosomes

Early endosomes are small fast moving heterogeneous compartments that are difficult to visualize. To better analyze interactions, larger endosomes were generated by high-level expression of the Ii or Rab5. The cytosolic tail of Ii is fusogenic and expression of Ii causes a prolonged endosomal pathway and enlargement of early endosomes (Engering et al., 1998; Nordeng et al., 2002; Romagnoli et al., 1993; Stang and Bakke, 1997). High-level expression of Rab5 has been found to increase endosome recruitment of EEA1 and enhance the early endosome fusion, resulting in larger endosomes (Bergeland et al., 2008; Gorvel et al., 1991; Li et al., 1995; Simonsen et al., 1998; Stenmark et al., 1994). cDNA for both molecules was subcloned into the inducible expression vector, pMep4, and as a reporter for the early endosomes we used the C-terminus of EEA1 (residues 1257–1411) fused to GFP (ctEEA1–GFP) (Bergeland et al., 2008; McBride et al., 1999). All constructs were stably

transfected into Madine-Darby canine kidney cells (MDCK) and human fibroblasts (M1 cells).

In control cells the diameter of the endosomes was 0.3–1 μm, however, 3–5 hours after Ii induction we observed frequent fusion events and a pronounced increase in size of the ctEEA1-positive vesicles (Fig. 1A, white arrow; supplementary material Movie 1). The characteristic diameter of endosomes 8 hours after induction was 2–4 μm, however, endosomes as large as 10 μm were observed. As the early endosomes fused and increased in size, there was a corresponding decrease in the number of small endosomes, indicating a transition to fewer and larger endosomes. Similar qualitative effects were observed in cells induced to express high levels of Rab5, with a corresponding transition to a reduced number of enlarged early endosomes (data not shown). The fusion between enlarged endosomes was rapid and completed within a few seconds as demonstrated in Fig. 1B.

Endosome fusion induces tubule formation and fission

In the endomembrane system there is a constant influx and efflux of membrane as a result of fusion and fission events. By following the homotypic fusions of the enlarged endosomal structures we detected tubular extensions coated with ctEEA1–GFP (Fig. 2A,D; supplementary material Movie 2). These dynamic tubular structures were especially apparent directly after fusion, seemingly as a direct consequence of the fusion. During the first minute after fusion we measured a 4.5-fold increase in tube formation from the endosomes (prior to fusion, 1.7±0.8 tubules per minute; after fusion, 7.8±2.6 tubules per minute; Fig. 2B). This particular tube formation subsequently decreased during the few minutes after fusion (Fig. 2B), if not followed by another fusion and a subsequent eruption of tubules. The average speed of the emerging tubes, measured after ten different fusions, was 0.9 μm/second, and they could stretch to as long as 10 μm. The tubules were dynamic and some could extend

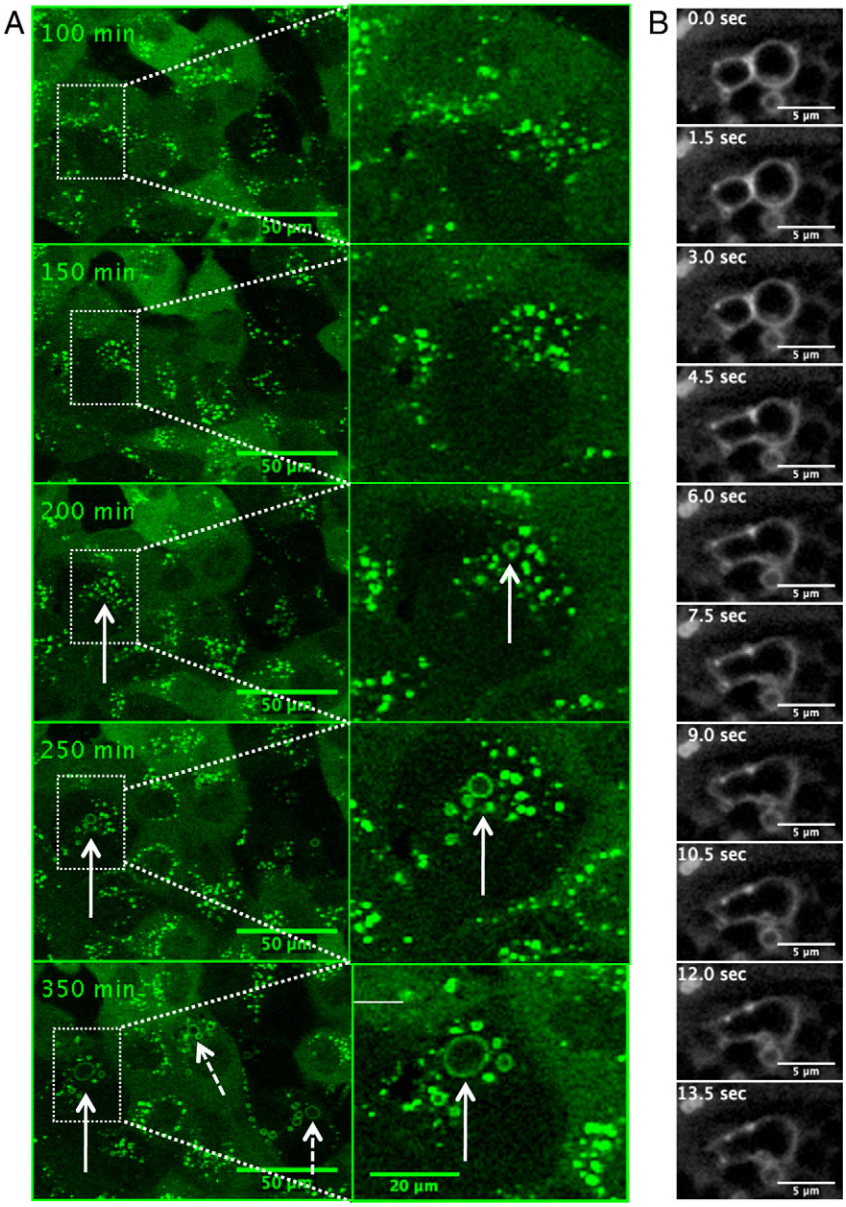

Fig. 1. Enlarged endosome formation and homotypic fusion. (**A**) MDCK cells stably transfected with CtEEA1–GFP and Ii-pMep4 were induced by $CdCl_2$ for 3 hours before image acquisition. A decrease in the number of early endosomes was observed upon the following enlargement of the endosomes. One specific endosomal enlargement is indicated by white arrows in the boxed regions, and dotted arrows point out similar enlargements. (**B**) One representative experiment, showing the fusion between enlarged early endosomes. The fusion pattern is rapid and the docking zone is fully opened in a few seconds.

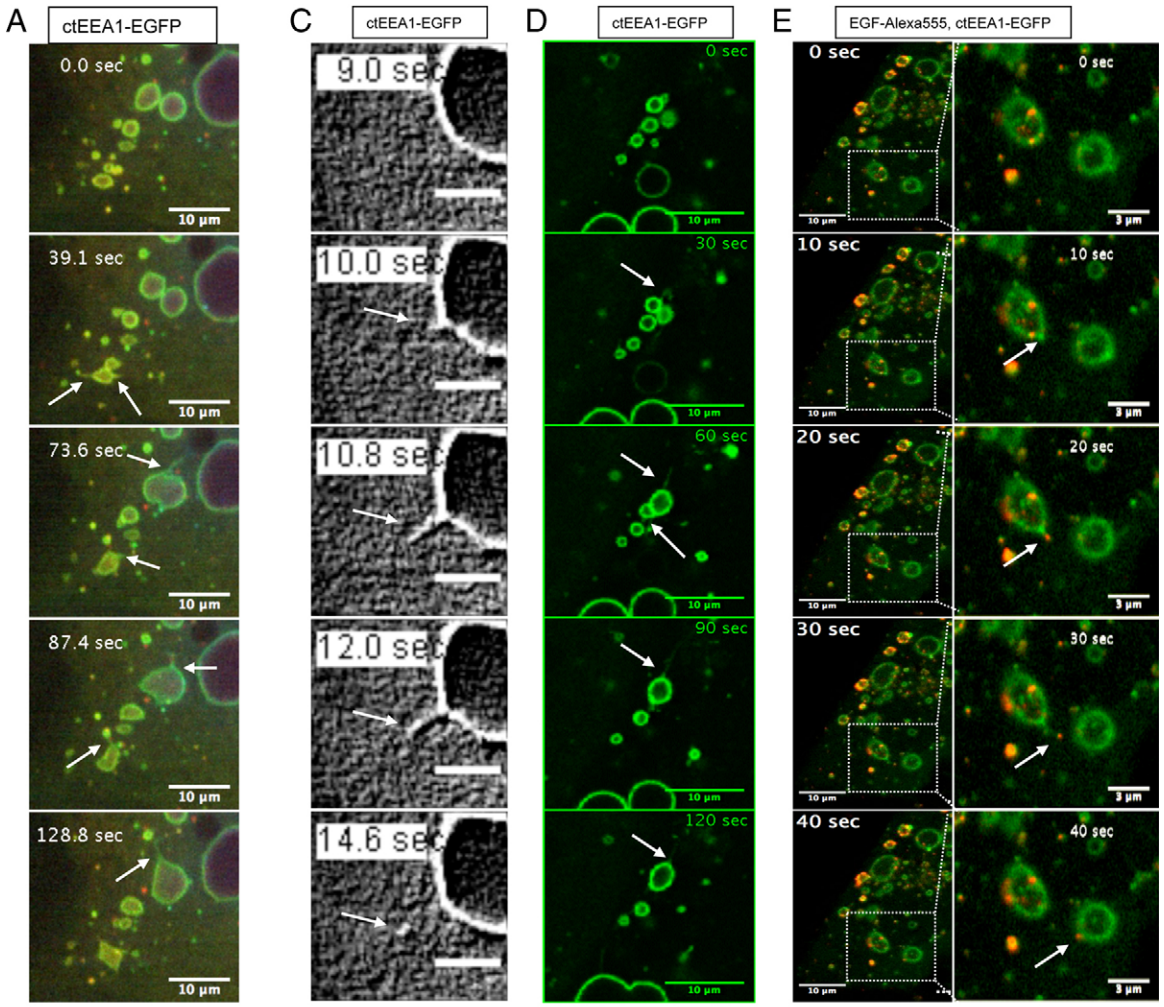

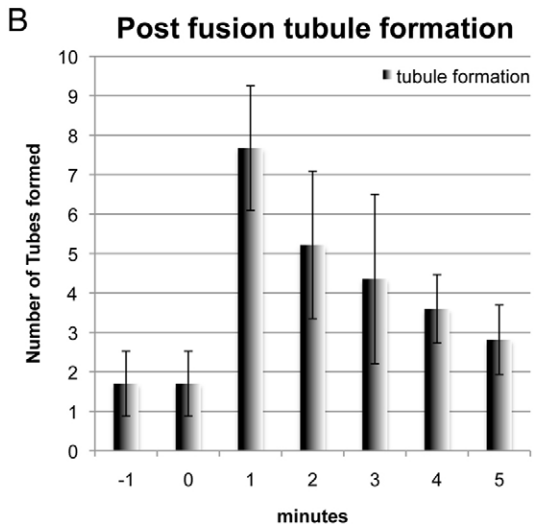

Fig. 2. Post-fusion tubule formation and fission. (**A**) Directly after fusion, many CtEEA1–GFP-positive emerging tubules were observed. This tube formation was visible on Ii- and Rab5-enlarged early endosomes. Ten *z*-slices were taken for each time point and were color coded: blue for the uppermost, green for the middle and red for the region close to the coverslip (see Materials and Methods). (**B**) The tube formation before and after fusion was calculated for ten different fusion couplets. (**C**) The tubular extensions also underwent full fission to form CtEEA1–GFP-positive vesicles (white arrows). Scale bars: 2 µm. (**D**) Post-fusion tubular extensions from Rab5-induced large endosomes. Time interval 30 seconds; four *z*-slices per time point are superimposed. (**E**) EGF–Alexa-Fluor-555 was added to M1 cells stably expressing Ii and ctEEA1 for 3 minutes prior to imaging. Internalized EGF localized to enlarged early endocytic structures. ctEEA1–GFP tubule formation positive for EGF–Alexa-Fluor-555 is indicated by white arrows. Time interval between frames is 10 seconds. Boxed regions are enlarged on the right.

and then disappear within 1 second, whereas others were more stable and could stay elongated for several seconds. By rapid four-dimensional (4-D) imaging we could also detect fission of the tubules as small free ctEEA1–GFP-positive vesicles (Fig. 2C; supplementary material Movie 3).

To study whether endocytic cargo could be transported through the tubules, Alexa-Fluor-555-labeled epidermal growth factor (EGF–Alexa-Fluor-555) was added to M1 cells stably expressing Ii and ctEEA1–GFP. Internalization was detected after 2 minutes and labeled EGF localized to early endosomes, where we subsequently observed accumulation of labeled EGF in microdomains on the enlarged endosomal structures (Fig. 2E; supplementary material Movie 4). Transport to the enlarged structures was observed to be through ctEEA1-positive vesicles or individual EGF-labeled vesicles (data not shown). Interaction of the incoming endosomes with the enlarged vesicles occurred through numerous fusion events and consequently numerous tubule formations were observed. The majority of the observed tubules formed were ctEEA1–GFP positive; however, 20±3.6% of the tubules contained EGF–Alexa-Fluor-555 (Fig. 2E, indicated by white arrows). We observed complete fission from the tubules, as shown in Fig. 2E. Apparently, EGF can be transported through these tubules and this can work as a transport step for proteins or receptors in early endosomes. Given that increased endosomal tubule formation and fission occurred immediately after fusion, this suggests that the fusion facilitates tubule formation and subsequent vesicular fission for intracellular vesicular transport.

Microtubules are essential for tubule formation and control the fusion rate

A working endosomal pathway depends on an intact cytoskeleton and endosomal transport is microtubule (MT) dependent (Nielsen et al., 1999). The average velocity of emerging tubules in our experiments was 0.9 μm/second, and this is in the range of the known speed of microtubule motors (Coy et al., 1999). To test for a link between emerging tubules and microtubule motors MDCK and M1 cells with enlarged Ii-induced endosomes were treated with the microtubule depolymerizing agent nocodazole. Independent experiments with MDCK cells stably transfected with tubulin–EYFP showed depolymerized microtubules when incubated with 10 μM nocodazole on ice for 45 minutes (data not shown). An impaired MT network did not inhibit fusion between the enlarged endosomes, on the contrary, the size of the early endosomes continued to grow dramatically, indicating an increased fusion activity (Fig. 3A; supplementary material Movie 5). In non-treated cells the average fusion rate of enlarged endosomes (diameter >2 μm) was 5±1.4 fusions per hour, whereas in cells treated with nocodazole the fusion rate was calculated to 16±3.9 fusions per hour (means ± s.d.; Fig. 3B). Interaction with microtubules thus seems to have regulatory effect on enlarged homotypic early endosome fusion.

Without intact microtubules the post-fusion, ctEEA1–GFP-positive tubular extensions were no longer observed. Instead, intralumenal ctEEA1–GFP-positive membrane extensions were detected and occasionally free ctEEA1–GFP-positive vesicles appeared in the endosomal lumen (Fig. 3C; supplementary material Movie 6). Consequently the dramatic increase in the size of early endosomes after depolymerization of microtubules is a result of both an increased fusion rate and impaired tubular fission.

Because a lack of intact microtubules leads to increased fusion of enlarged endosomes this effect should also be visible studying normal sized endosomes. We therefore performed identical experiments as above but the MDCK cells were transfected with ctEEA1–GFP alone. After nocodazole treatment, the spatial distribution changed and the EEA1-positive endosomes moved to the cell periphery, as expected because the microtubules were no longer intact. Moreover, the size of the ctEEA1–GFP-positive vesicles increased rapidly by active fusion (becoming three to four times larger than their original size), and no tubule formation or fission was observed after fusion (Fig. 3D; supplementary material Movie 7). Together, our data indicate that microtubules regulate endosome fusion and fission processes independently of vesicle size.

Kif16b and dynein control the post-fusion tubule formation

It is well known that the microtubule-associated motors kinesin and dynein control vesicular trafficking and tubule formation (Bourekas et al., 1999; Roux et al., 2002; Verhey and Hammond, 2009). Having established a role for microtubules in tubular formation we decided to investigate the role of specific microtubule motors already shown to have a role in trafficking of early endosomes. Kif5B, a kinesin-1 family member, is important for peripheral distribution of early endosomes, as well as endosome fission (Loubery et al., 2008; Nath et al., 2007). We constructed a mutant known to inhibit kinesin-1 function encompassing the first 330 amino acids of the human Kif5b fused to EGFP (Schepis et al., 2007), which we named mutKif5b. This mutant was transfected into MDCK cells expressing Ii-induced enlarged endosomes. In cells positive for mutKif5b–EGFP we observed that mitochondria changed from being uniformly distributed in the cytoplasm to become more clustered in the perinuclear region, which did not occur in control cells (Fig. 4A). This is an established effect of knocking down Kif5b (Tanaka et al., 1998) and indicated a successful inhibition of Kif5b activity. For an early endosomal marker the cells were transfected with ctEEA1–mRFP or Rab5–mCherry. After transfection of mutKif5b, the cells still had enlarged endosomes and the endosomal localization was not specifically altered. Fusions and extensive tubule formations were still observed, indicating that Kif5B is not required for the specific Rab5- or EEA1-positive post-fusion tubule formation (Fig. 4B,C; supplementary material Movie 8, data for ctEEA1–GFP is not shown).

Another candidate for pulling the post-fusion tubules is the endosome-binding microtubule motor Kif16b that belongs to the kinesin-3 family. Kif16b was reported to be responsible for movement of early endosomes on microtubules (Hoepfner et al., 2005). Two different YFP constructs, the wild-type Kif16B–YFP and the dominant-negative mutant Kif16B–S109A–YFP, were transfected into MDCK cells. Whereas both fusion proteins were localized to Rab5–mCherry-positive early endosomal vesicles, the wild-type one localized more to the cell periphery and the mutant to the perinuclear area, as reported earlier (Hoepfner et al., 2005) (Fig. 5A,C). The post-fusion Kif16B–YFP-positive tubules increased dramatically after fusion (Fig. 5A–C; supplementary material Movies 9 and 10), from 1.2±0.8 tubules per minute before fusion, to 8.2±2.6 tubules per minute in the first minute after fusion (Fig. 5D). In cells expressing the mutant Kif16B-S109A–YFP, by contrast, hardly any tubules were visible after fusion (Fig. 5C,D; supplementary material Movie 11). The serine to alanine mutation in Kif16B has

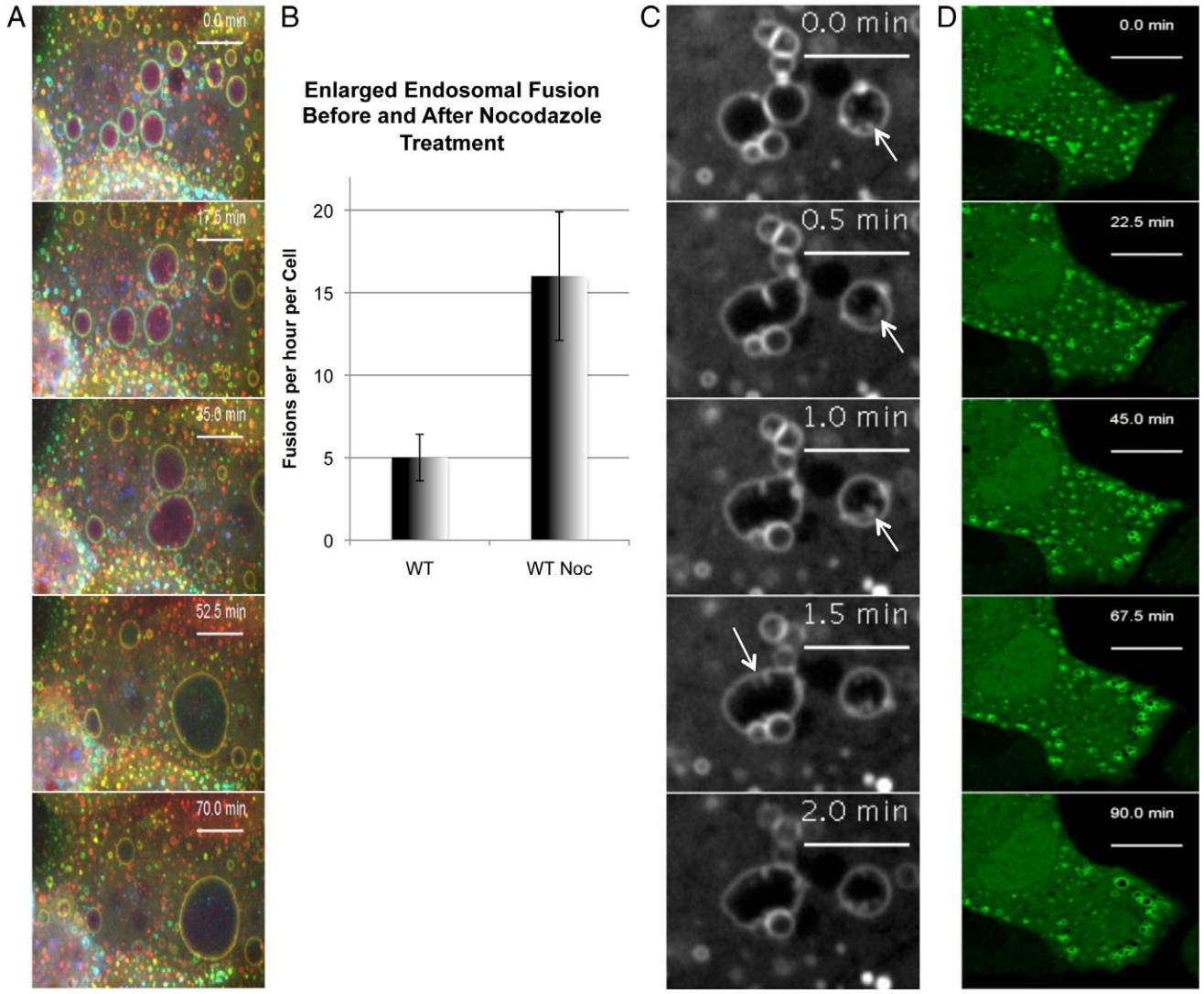

Fig. 3. Microtubular control of early endosome size and tubule formation. (**A**) Cells expressing CtEEA1–GFP and Ii were treated with nocodazole and increased fusion and further enlargement of endosomes was observed. Representative images at various time points after adding nocodazole are shown and ten *z*-slices were taken at every time point. Images are color coded as in Fig. 2A. Scale bars: 10 µm. (**B**) Endosomal fusions per hour were calculated for endosomes larger than 2 µm in diameter. (**C**) No tubules were observed after fusion in cells treated with nocodazole. Instead inward budding and intralumenal CtEEA1–GFP-positive structures were observed (white arrows). Scale bars: 5 µm. (**D**) MDCK cells stably transfected with CtEEA1–GFP lacking the enlarged endosomes were subjected to similar nocodazole treatment as in the previous experiment. Depolymerizing the microtubules induces enlargement of the ctEEA1–GFP-labeled endosomes similar to enlarged endosomes. Scale bars: 10 µm.

been shown to impair its motor activity and the GFP fusion protein has a dominant-negative effect on the endogenous motor (Nakata and Hirokawa, 1995). Because tubulation after fusion was barely observed in cells expressing the Kif16B mutant this indicates an active role for Kif16B in pulling the tubules on microtubule tracks.

Post-fusion tubules were either Rab5–mCherry positive, Kif16b–YFP positive or labeled with both markers (examples of the different types are indicated by colored arrows in Fig. 5B). The three different tubules signified by the two markers, gives an indication of a complex tubular fission system. An additional interesting observation was that Kif16b-positive tubules predominantly elongated toward, and possibly made contact with, adjacent Kif16b–YFP-positive endosomes (Fig. 5A; supplementary material Movie 9).

A further molecular motor found to be involved in controlling the trafficking of early endosomes is the dynein–dynactin complex (Burgess et al., 1999; Driskell et al., 2007). To test whether this complex is involved in tubule formation we transfected the dominant-negative mutant of dynactin in which the coiled-coil-1 (CC1) region of the $p150^{glued}$ subunit (also known as dynactin subunit 1, DCTN1) was fused to monomeric RFP (CC1–mRFP) (Driskell et al., 2007). As a control for the CC1 dynein inhibition, MDCK cells were transfected with CC1–mRFP and labeled for anti-GM130, a Golgi marker. We could clearly detect a fragmented Golgi network in these cells, which was not seen in control cells transfected with wt–mRFP (Fig. 6A), evidence for the functionality of the construct (Christoforidis et al., 1999b). MDCK cells stably transfected with ctEEA1–GFP and Ii were induced to express Ii for 24 hours,

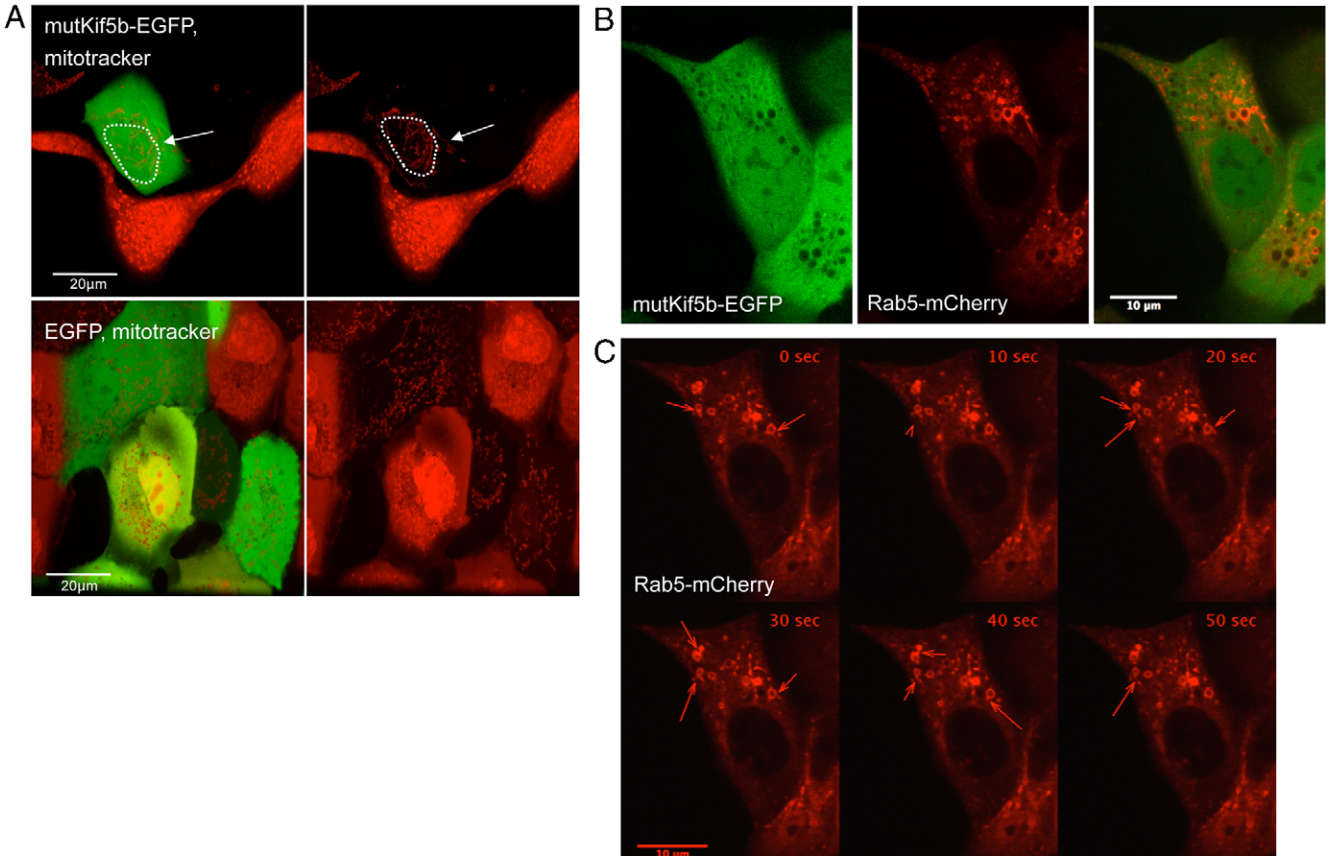

Fig. 4. MutKif5b does not inhibit formation Rab5-positive tubules. (**A**) Control experiment shows an inhibition of Kif5b by altering the localization of mitochondria (labeled with Mitotracker; red). White arrow indicates relocation of mitochondria to the perinuclear area. (**B**) MDCK cells transfected with mutKif5–EGFP and Rab5–mCherry were followed over time to identify tubule formation. The images show the cells represented in the subsequent time series, shown in C. (**C**) A maximum projection from supplementary material Movie 8 with 10 seconds between frames, showing extensive Rab5–mCherry tubulation (red arrows) after transfection.

resulting in the formation of many enlarged endosomes. These cells were then transiently transfected for 18 hours with CC1–mRFP or with mRFP as a control. In cells transfected with CC1–mRFP we could clearly observe fewer enlarged endocytic structures compared with control cells (Fig. 6B). By calculating the fraction of cells with enlarged endosomes, we identified a specific difference between CC1-transfected cells and control cells. Enlarged endosomes were found in 70.3% mRFP control cells, but only 25.4% of the cells transfected with CC1–mRFP contained enlarged endosomes (Fig. 6). Thus, our data indicate that the dynein motor is also involved in controlling the size of the enlarged early endosomes.

In the 25.4% of CC1–mRFP-transfected cells with enlarged endosomes we observed intraluminal ctEEA1–GFP-positive structures in the enlarged vesicles (Fig. 6E, white arrows). This is similar to the situation when the microtubules were depolymerized and there were no tubules formed after fusion (Fig. 3B, white arrows). This result indicates that tubule formation was inhibited and provides further evidence that dynein is involved in the formation of tubules.

Discussion

In this work we took advantage of two different mechanisms to increase the size of the early endosomes in order to gain new insight into the dynamic interactions of these organelles in live cells. The fusion pattern of vesicles in living cells has previously been divided into ‘explosive’ and ‘bridge’ fusion (Roberts et al., 1999). In explosive fusion there is a rapid merger of vesicle membranes, leading to the formation of a single, enlarged compartment. In bridge fusion membrane merger proceeds slowly, and the transfer of membrane from the donor to the acceptor endosomal vesicle appears to occur entirely through a very narrow bridge between fusion pairs (Roberts et al., 1999). The fusion of the EEA1-positive endosomes observed in our experiments can then be described as explosive, because it is completed in a few a seconds. The more slow bridge fusion probably represents a fusion event taking place in later stages in the endocytic pathway (Roberts et al., 1999), and was not observed in our experiments.

Subsequent to the rapid early fusion of endosomes we were able to visualize and calculate extensive emergence of thin ctEEA1–GFP-coated tubules from various parts of the newly formed organelle. From Fig. 2B we can see that there are tubes being formed without a ‘detectable’ preceding fusion. This is an expected result because we cannot detect all the incoming fusions of smaller vesicles that characterize the tube formation background. From the very tip of the tubules we observed small, ctEEA1–GFP vesicles pinching off. We were not able to follow these vesicles for long, and could not detect their target membrane. However, after uptake of EGF–Alexa-Fluor-555 we

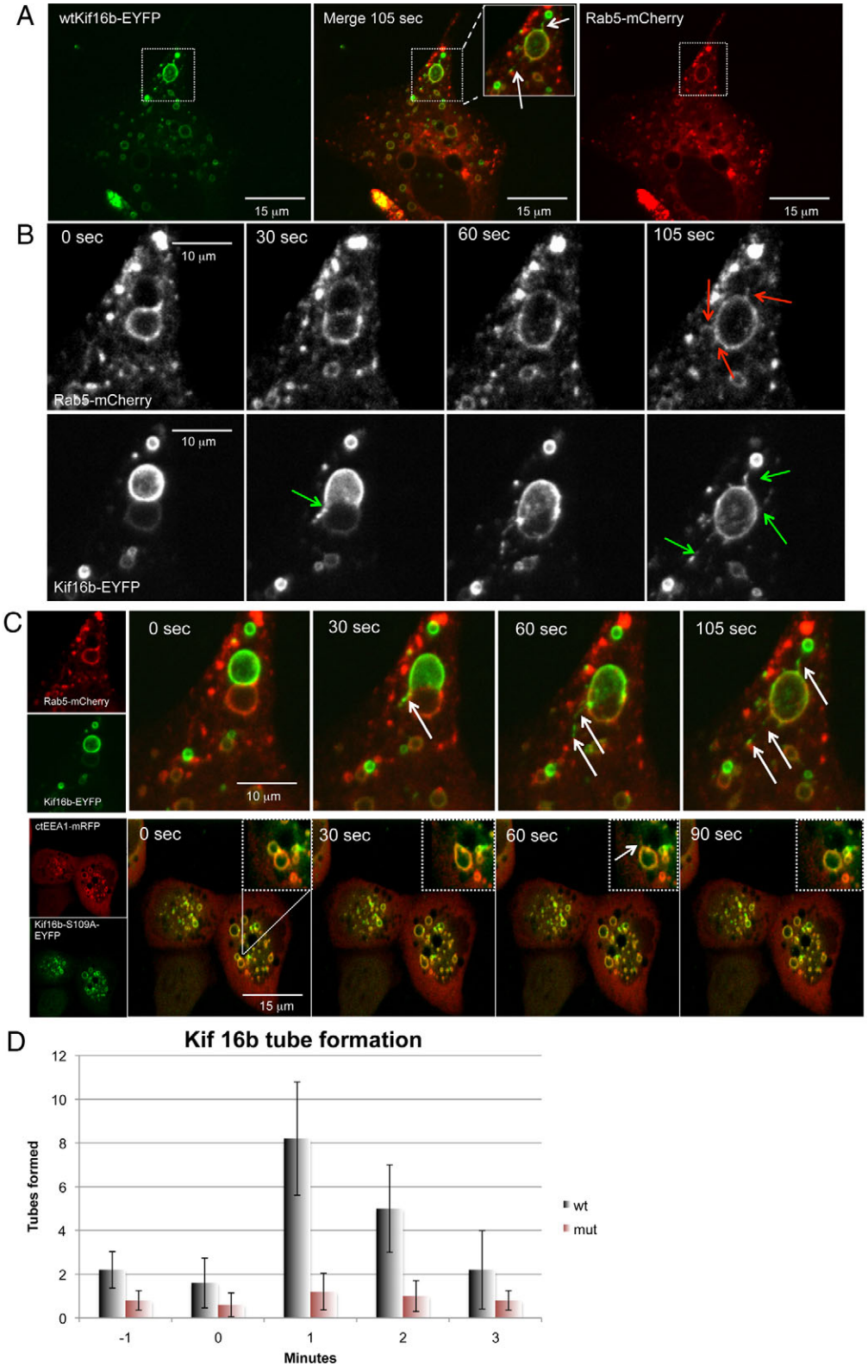

Fig. 5. Formation of post-fusion Kif16b-positive tubules. (**A**,**B**) MDCK cells stably transfected with Ii were cotransfected with Rab5–mCherry and wtKif16b–YFP. Partially membranous colocalizations were observed before and after fusion. Formation of post-fusion tubules occurred from enlarged endosomal structures (see enlarged inset in A; supplementary material Movie 9). Kif16b tubules stretched predominantly in the direction of other Kif16b-positive endosomes (white arrows in the inset). Image rendering used a maximum projection of six *z*-slices per time point. Panel B shows a time frame of the tubule formation occurring in A. Time frames show Rab5–mCherry, wtKif16b–YFP tubule formation after fusion. The colored arrows indicate different tubule formations positive for either Rab5–mCherry or Kif16b–YFP. (**C**) The MDCK cells were transfected with Kif16B-S109A–YFP a dominant-negative mutant and ctEEA1–mRFP. The figure shows a comparison between post-fusion tubule formation of the wild type (same as B) and the mutant. In the wild type the tubule formation is evident (white arrows). In the dominant mutant early endosomes had a more perinuclear localization and very few to no post-fusion tubules. A representative fusion of an early endosome positive for Kif16B-S109A–YFP is shown in the inset, in which one tube was detected. (**D**) Similar calculations as in Fig. 3B were made and tubule formations were counted before and after fusion of five random couplets. Post-fusion tubule formation is seven-fold higher in wtKif16b–YFP than the mutant, Kif16B-S109A–YFP.

found that only a specific fraction (1/5) of the EEA1-positive, post-fusion tubules contained the fluorescent EGF. These structures appeared to reflect a transport of cargo between early endosomal vesicles or towards the plasma membrane. EGF stimulation of EGF receptors directs the majority of the receptors to lysosomal degradation, although some are recycled (Roepstorff et al., 2009). Whether this is a specific tubular sorting of the EGF receptors alone is not possible to predict through our experimental setup. However, our observations indicate a transport option for cargo or the EGF receptor,

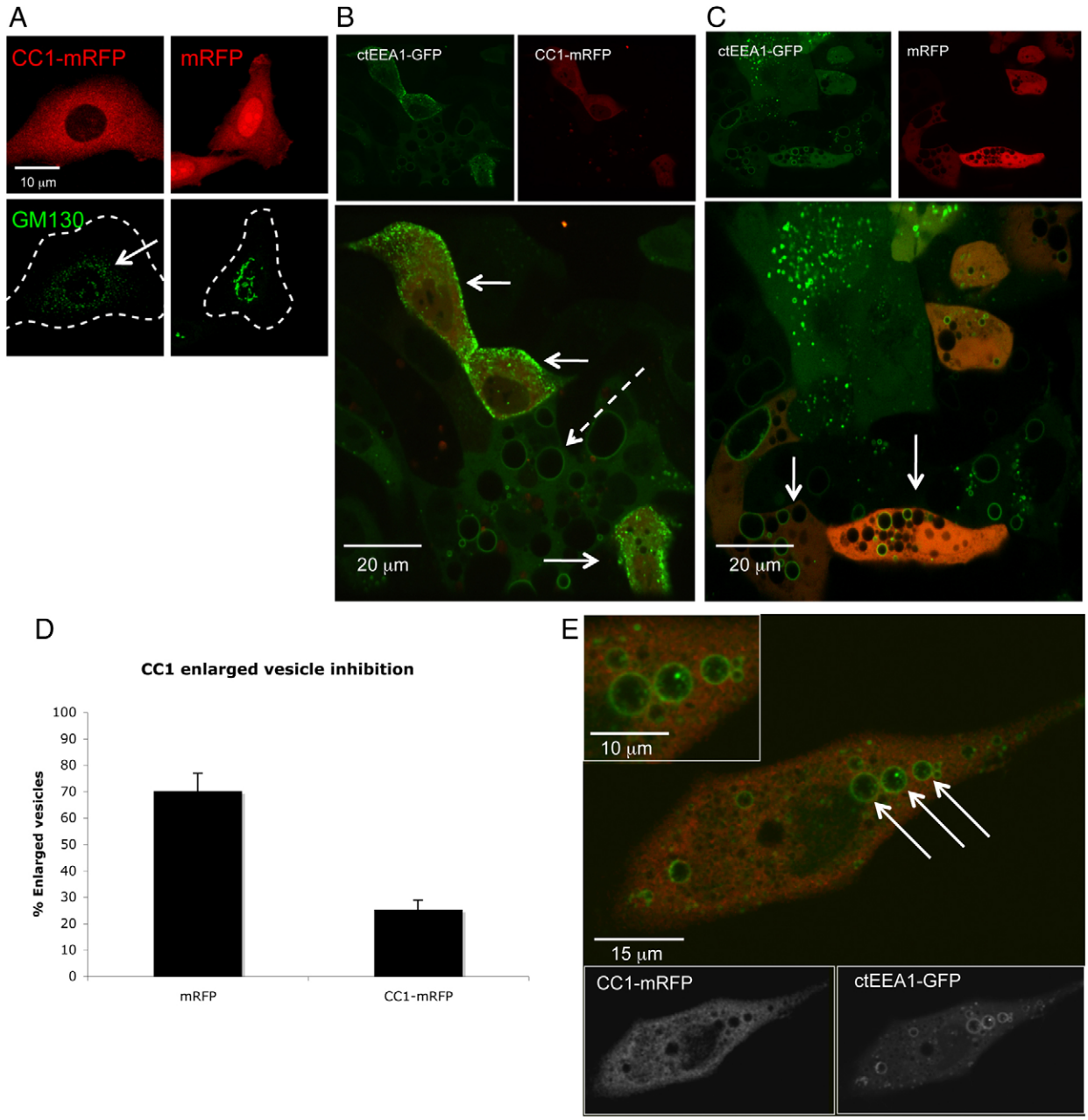

Fig. 6. Dynein controls enlarged endosome morphology. (**A**) MDCK cells were transfected with CC1–mRFP, and as a control for dynein inhibition the Golgi network was labeled with an antibody recognizing GM130 (green). The dispersal of the Golgi network (white arrow) seen in the mutant implies an inhibition of the dynein–dynactin complex. Dashed lines represent the PM. (**B**,**C**) MDCK cells stably expressing Ii and ctEEA1–EGFP. The cells were either transfected with CC1–mRFP (B) or mRFP (C) and Ii was induced with $CdCl_2$ overnight. Typical endosomal morphology after CC1 expression is indicated by white arrows and untransfected neighboring cells with enlarged endosomes are indicated by a dashed white arrow. In control calls the endosomal morphology was unaltered (white arrows, C). (**D**) Percentage of cells with enlarged vesicles 18 hours post transfection. 20 culture areas were counted representing 70 cells (values are means ± s.d.). (**E**) A CC1-transfected cell with formation of intralumenal invaginations (white arrows) upon inhibition of dynein.

concentrating them into tubules either for recycling or sorting within the endocytic pathway.

The stimulus for the extensive tubule formation may be that when two vesicles with identical volume fuse, the newly formed vesicle has 20% excess membrane, regardless of vesicle size (Pantazatos and MacDonald, 1999). This additional membrane has to be removed in order to balance the surface to volume ratio after fusion, which could be achieved by tubule formation. Even more importantly, the addition of membrane upon fusion also destabilizes the endosomal membrane, and subsequently lowers the force barrier connected with the initial deformation of the membrane (Koster et al., 2005). Molecular motors can utilize this transient instability in the membrane to form a tubule.

By depolymerizing the microtubules we removed the intracellular highways required for trafficking, fusion and fission (Murray and Wolkoff, 2003). Subsequent to the

depolymerization of the microtubules no tubules were observed after fusion. On the contrary, we observed both tubular and vesicular intralumenal structures, reminiscent of observations made during in vitro experiments (Pantazatos and MacDonald, 1999). We hypothesize, that by depolymerizing the microtubules the excess membrane presumably invaginates into the luminal space in order to maintain the surface to volume equilibrium.

The average formation speed of the fusion-induced tubules was calculated to be similar to established vesicular trafficking speed along the microtubules (Coy et al., 1999), and the fusion tubules were indeed found to be dependent on intact microtubules. When microtubules were depolymerized by nocodazole treatment we additionally observed an increase in the endosomal fusion rate, concomitant with a further increase in the size of the already enlarged endocytic structures (Fig. 3A). This is a dual effect of increased fusion rate and obstruction of tubule formation and fission. Furthermore, a similar effect was detected with ctEEA1–GFP in normal sized endosomes in control cells (Fig. 3C). Our observations indicate that the strict microtubule control of endosomal fusion and fission is similar in cells with enlarged endosomes as in unperturbed cells.

Two families of kinesins have been found to interact with the early endocytic compartments, kinesin 1 and kinesin 3 (Hirokawa et al., 2009). We were specifically interested in Kif5b and Kif16b, both known to be involved in early endosomal trafficking and tubule formation (Hoepfner et al., 2005; Nath et al., 2007). High expression of the Kif5b mutant altered mitochondrial localization but had no observable effect on tubule formation. By contrast, we found that Kif16b–YFP localized to three different classes of post-fusion emerging tubules: Kif16b-YFP-positive tubules, Rab5–mCherry-positive tubules, and tubules positive for both Kif16b–YFP and Rab5–mCherry. This demonstrates the complexity of the sorting and trafficking from the early endocytic compartment. Expression of the mutant Kif16b inhibited post-fusion tubule formation and confirmed a specific role for KIf16b in tubule formation. Additionally, the most prominent tubules observed in the experiment were Kif16b–YFP positive. These tubules predominantly interact with Kif16b–YFP-positive early endosomes and presumably characterize an endosomal tubular cargo sorting induced by fusion.

The minus-end motor dynein was also demonstrated to be involved in regulating the size of the enlarged endosomes. In cells expressing CC1–mRFP of the dynactin p150^{glued}, the dynein–dynactin motor complex is impaired (Driskell et al., 2007). Only 25.4% of these cells contained enlarged endosomes, much less than in control cells, indicating impaired fusion and fission coordination. Additionally, we found ctEEA1–GFP-positive, enlarged multivesicular bodies in cells expressing CC1–mRFP, but empty enlarged endosomes in control cells expressing mRFP. This suggests impaired fission after fusion, similar to what we observed when the cells were incubated with nocodazole. Dynein has been shown to facilitate fusion of early endosomes (Driskell et al., 2007) and combined with our data this indicates that dynein plays a dual role facilitating both fusion and fission.

In conclusion, we show, through live cell experiments, a casual link between fusion and fission, where fusion functions as a membrane-destabilizing factor, facilitating spontaneous tubule formation and fission, controlled by molecular motors.

Materials and Methods

DNA constructs

Complementary DNAs encoding CD74 (Bakke and Dobberstein, 1990) and Rab5 (Chavrier et al., 1990) have been described previously. These were subcloned into the pMep4 vector (Invitrogen) as *Kpn*I–*Bam*HI and *Hin*dIII–*Xho*I fragments, respectively (Gregers et al., 2003). ctEEA1–GFP has been previously described (Christoforidis et al., 1999a; Lawe et al., 2002; McBride et al., 1999).

Rab5–mCherry was made by amplifying Rab5 and mCherry separately by PCR using the following primers: for Rab5, 5′-AGAGA**GGATCC**ATGGCTAG-TCGAGGCGCAAC-3′ (the *Bam*HI site is in bold) and 5′-AGAGA**CTCG-AG**TTAGTTACTACAACACTG-3′ (*Xho*I site is in bold); for mCherry, 5′-AGAGA**GGTACC** ATGGTGAGCAAGGGCGAGGAG-3′ (*Kpn*I site) and 5′-AGAGA**GGATCC**CTTGTACAGCTCGTCCATGCC-3′ (*Bam*HI site). mCherry was ligated to the N-terminus of Rab5 by the *Bam*HI site and subsequently subcloned into the pcDNA3 vector (Invitrogen) at the *Kpn*I and *Xho*I sites.

The primer pair 5′-GCTCAGAATTCATGGCGGACCTGGCC-3′ and 5′-CAGATGGGCCCGACAAACTGTGTTCTTAATTGTTTTGG-3′ was used to amplify the coding sequence for the first 330 N-terminal amino acids of human KIF5B. PCR products were ligated into pEGFP-N1 (Clontech) using the *Eco*RI and *Apa*I restriction sites. Cells grown on 12 mm glass coverslips were transfected with plasmid DNA using FuGENE 6 (Roche) according to the manufacturer's protocol. KIF16B–YFP and KIF16B-S109A–YFP were kindly provided by Marino Zerial (Max Plack Institute of Molecular Cell Biology and Genetics Dresden, Germany) and used as described previously (Hoepfner et al., 2005). CC1–mRFP was kindly provided by Viki Allan (University of Manchester Faculty of Life Sciences, UK).

Cell culture

Madine-Darby canine kidney strain II (MDCK) and M1 (human fibroblasts) cells were stably transfected with Ii, Rab5-pMep4 and ctEEA1–EGFP. Ii and Rab5 expression was induced by the addition of 25 μM $CdCl_2$ in MDCK cells and 5 μM in M1 cells. The cells were grown in complete medium: DMEM (Bio Whittaker) supplemented with 9% FCS (Integro), 2 mM glutamine, 25 U/ml penicillin and 25 μg/ml streptomycin (all from Bio Whittaker) in 6% CO_2 in a 37℃ incubator.

Expression of protein and uptake of EGF

Stably transfected MDCK cells were grown in chambered coverglasses (Nalgene and Mattek), incubated with DMEM at 37℃ overnight. The cells were incubated with $CdCl_2$ for between 6 and 12 hours. Immediately before imaging the cells were washed with PBS and then incubated with microscopy medium: DMEM without Phenol Red and sodium carbonate, supplemented with 3.5 g/l D-glucose to a final concentration of 4.5 g/l; 25 mM HEPES, adjusted to pH 7.5 (Bergeland et al., 2001), plus 10% FCS. EGF–Alexa-Fluor-555 (Molecular Probes) was added to the live cells on the microscope, at a final concentration of 100 ng/ml.

Confocal microscopy

For fast and 4-D imaging, a Perkin Elmer Ultra View LCI/RS and Andor Revolution XD spinning disc microscope was used with an Olympus IX 71 with a PlanApo N 60×/1.42 NA oil immersion objective. The CSU22 spinning disc unit was synchronized with an iXon^{EM+} 885 EMCCD camera. A stable cellular environment was maintained with a 37℃ microscope chamber (Solent Scientific, Segensworth, UK).

The LCI system was equipped with a NikonEclipse TE 2000 microscope with an Astro Cam Ultra Pix CCD camera. Nikon Plan Fluotar, 100×1.30 NA oil immersion objective, and the RS scanning system was equipped with a Zeiss Axiovert 200 with a 63×/1.40 NA oil immersion objective and a Hammamatsu Ocra ER cooled CCD camera. Spinning disc technology, provided by Nipkow (http://www.yokogawa.com/scanner/products/csu22e.htm), used a multiple pinhole disc. Exposure time varied from 20 to 500 ms depending on the purpose of the experiment and sample intensity. Samples were exited with an argon–krypton, argon ion laser using the 488/568 lines.

Movie editing and quantitative immunofluorescence analysis

For movie and image analysis, Imaris (Bitplane) and ImageJ software was used. The elongation speed was calculated from ten different experiments showing post-fusion tubule formations. ImageJ was used to manually track and calculate the speed of tubule elongation.

Projections and color-coded movies were produced with a macro written in IDL 5.5 (http://www.exelisvis.com/language/en-US/ProductsServices/IDL.aspx) by Timo Zimmermann, EMBL. The color-coded projection is in three colors: blue for the uppermost *z*-slices to the top of the cells, green for the middle and red for the region close to the coverslip.

Chemicals and inhibitors

Nocodazole (Sigma) were dissolved in dimethyl sulfoxide (DMSO) at concentrations of 10 μM. After the drug was diluted in cultures, the final concentration of DMSO never exceeded 1% (vol/vol). Nocodazole was added to

the sample 30 minutes after incubation on ice, the rest of the reagents were added when the sample was on the microscope stage.

Acknowledgements

We thank Anne Simonsen and Gareth Griffiths for fruitful discussions and critically reading the manuscript. We also thank the Advanced Light Microscopy Facility at the EMBL Heidelberg and the Molecular Imaging Centre at the University of Bergen for the use of their instrumentation in the early stages of the project. The major part of the work was performed at the NorMIC Oslo imaging platform, University of Oslo.

Funding

This work was supported by the Norwegian Cancer Society; and the Norwegian Research Council; and EU Grant Microban [EU network no MRTN-CT-2003-504227 to O.B. and S.S.].

Supplementary material available online at
http://jcs.biologists.org/lookup/suppl/doi:10.1242/jcs.092569/-/DC1

References

Bakke, O. and Dobberstein, B. (1990). MHC class II-associated invariant chain contains a sorting signal for endosomal compartments. *Cell* **63**, 707-716.

Bergeland, T., Widerberg, J., Bakke, O. and Nordeng, T. W. (2001). Mitotic partitioning of endosomes and lysosomes. *Curr. Biol.* **11**, 644-651.

Bergeland, T., Haugen, L., Landsverk, O. J., Stenmark, H. and Bakke, O. (2008). Cell-cycle-dependent binding kinetics for the early endosomal tethering factor EEA1. *EMBO Rep.* **9**, 171-178.

Bourekas, E. C., Christoforidis, G. A., Abduljalil, A. M., Kangarlu, A., Chakeres, D. W., Spigos, D. G. and Robitaille, P. M. (1999). High resolution MRI of the deep gray nuclei at 8 Tesla. *J. Comput. Assisted Tomogr.* **23**, 867-874.

Burgess, R. E., Yu, Y., Christoforidis, G. A., Bourekas, E. C., Chakeres, D. W., Spigos, D., Kangarlu, A., Abduljalil, A. M. and Robitaille, P. M. (1999). Human leptomeningeal and cortical vascular anatomy of the cerebral cortex at 8 Tesla. *J. Comput. Assisted Tomogr.* **23**, 850-856.

Buss, F., Arden, S. D., Lindsay, M., Luzio, J. P. and Kendrick-Jones, J. (2001). Myosin VI isoform localized to clathrin-coated vesicles with a role in clathrin-mediated endocytosis. *EMBO J.* **20**, 3676-3684.

Chavrier, P., Parton, R. G., Hauri, H. P., Simons, K. and Zerial, M. (1990). Localization of low molecular weight GTP binding proteins to exocytic and endocytic compartments. *Cell* **62**, 317-329.

Christoforidis, S., McBride, H. M., Burgoyne, R. D. and Zerial, M. (1999a). The Rab5 effector EEA1 is a core component of endosome docking. *Nature* **397**, 621-625.

Christoforidis, S., Miaczynska, M., Ashman, K., Wilm, M., Zhao, L., Yip, S. C., Waterfield, M. D., Backer, J. M. and Zerial, M. (1999b). Phosphatidylinositol-3-OH kinases are Rab5 effectors. *Nat. Cell Biol.* **1**, 249-252.

Clague, M. J. (1998). Molecular aspects of the endocytic pathway. *Biochem. J.* **336**, 271-282.

Coy, D. L., Wagenbach, M. and Howard, J. (1999). Kinesin takes one 8-nm step for each ATP that it hydrolyzes. *J. Biol. Chem.* **274**, 3667-3671.

Driskell, O. J., Mironov, A., Allan, V. J. and Woodman, P. G. (2007). Dynein is required for receptor sorting and the morphogenesis of early endosomes. *Nat. Cell Biol.* **9**, 113-120.

Engering, A. J., Richters, C. D., Fluitsma, D. M., van Pelt, A. M., Kamperdijk, E. W., Hoefsmit, E. C. and Pieters, J. (1998). MHC class II and invariant chain biosynthesis and transport during maturation of human precursor dendritic cells. *Int. Immunol.* **10**, 1713-1723.

Gorvel, J. P., Chavrier, P., Zerial, M. and Gruenberg, J. (1991). rab5 controls early endosome fusion in vitro. *Cell* **64**, 915-925.

Gregers, T. F., Nordeng, T. W., Birkeland, H. C., Sandlie, I. and Bakke, O. (2003). The cytoplasmic tail of invariant chain modulates antigen processing and presentation. *Eur. J. Immunol.* **33**, 277-286.

Gruenberg, J., Griffiths, G. and Howell, K. E. (1989). Characterization of the early endosome and putative endocytic carrier vesicles in vivo and with an assay of vesicle fusion in vitro. *J. Cell Biol.* **108**, 1301-1316.

Hirokawa, N., Noda, Y., Tanaka, Y. and Niwa, S. (2009). Kinesin superfamily motor proteins and intracellular transport. *Nat. Rev. Mol. Cell Biol.* **10**, 682-696.

Hoepfner, S., Severin, F., Cabezas, A., Habermann, B., Runge, A., Gillooly, D., Stenmark, H. and Zerial, M. (2005). Modulation of receptor recycling and degradation by the endosomal kinesin KIF16B. *Cell* **121**, 437-450.

Koster, G., Cacciuto, A., Derenyi, I., Frenkel, D. and Dogterom, M. (2005). Force barriers for membrane tube formation. *Phys. Rev. Lett.* **94**, 068101.

Lawe, D. C., Chawla, A., Merithew, E., Dumas, J., Carrington, W., Fogarty, K., Lifshitz, L., Tuft, R., Lambright, D. and Corvera, S. (2002). Sequential roles for phosphatidylinositol 3-phosphate and Rab5 in tethering and fusion of early endosomes via their interaction with EEA1. *J. Biol. Chem.* **277**, 8611-8617.

Li, G., D'Souza-Schorey, C., Barbieri, M. A., Roberts, R. L., Klippel, A., Williams, L. T. and Stahl, P. D. (1995). Evidence for phosphatidylinositol 3-kinase as a regulator of endocytosis via activation of Rab5. *Proc. Natl. Acad. Sci. USA* **92**, 10207-10211.

Lippincott-Schwartz, J., Roberts, T. H. and Hirschberg, K. (2000). Secretory protein trafficking and organelle dynamics in living cells. *Annu. Rev. Cell Dev. Biol.* **16**, 557-589.

Loubery, S., Wilhelm, C., Hurbain, I., Neveu, S., Louvard, D. and Coudrier, E. (2008). Different microtubule motors move early and late endocytic compartments. *Traffic* **9**, 492-509.

McBride, H. M., Rybin, V., Murphy, C., Giner, A., Teasdale, R. and Zerial, M. (1999). Oligomeric complexes link Rab5 effectors with NSF and drive membrane fusion via interactions between EEA1 and syntaxin 13. *Cell* **98**, 377-386.

Morris, S. M., Arden, S. D., Roberts, R. C., Kendrick-Jones, J., Cooper, J. A., Luzio, J. P. and Buss, F. (2002). Myosin VI binds to and localises with Dab2, potentially linking receptor-mediated endocytosis and the actin cytoskeleton. *Traffic* **3**, 331-341.

Mukherjee, S. and Maxfield, F. R. (2000). Role of membrane organization and membrane domains in endocytic lipid trafficking. *Traffic* **1**, 203-211.

Murray, J. W. and Wolkoff, A. W. (2003). Roles of the cytoskeleton and motor proteins in endocytic sorting. *Adv. Drug Deliv. Rev.* **55**, 1385-1403.

Nakata, T. and Hirokawa, N. (1995). Point mutation of adenosine triphosphate-binding motif generated rigor kinesin that selectively blocks anterograde lysosome membrane transport. *J. Cell Biol.* **131**, 1039-1053.

Nath, S., Bananis, E., Sarkar, S., Stockert, R. J., Sperry, A. O., Murray, J. W. and Wolkoff, A. W. (2007). Kif5B and Kifc1 interact and are required for motility and fission of early endocytic vesicles in mouse liver. *Mol. Biol. Cell* **18**, 1839-1849.

Nielsen, E., Severin, F., Backer, J. M., Hyman, A. A. and Zerial, M. (1999). Rab5 regulates motility of early endosomes on microtubules. *Nat. Cell Biol.* **1**, 376-382.

Nordeng, T. W., Gregers, T. F., Kongsvik, T. L., Meresse, S., Gorvel, J. P., Jourdan, F., Motta, A. and Bakke, O. (2002). The cytoplasmic tail of invariant chain regulates endosome fusion and morphology. *Mol. Biol. Cell* **13**, 1846-1856.

Pantazatos, D. P. and MacDonald, R. C. (1999). Directly observed membrane fusion between oppositely charged phospholipid bilayers. *J. Membr. Biol.* **170**, 27-38.

Peter, B. J., Kent, H. M., Mills, I. G., Vallis, Y., Butler, P. J., Evans, P. R. and McMahon, H. T. (2004). BAR domains as sensors of membrane curvature: the amphiphysin BAR structure. *Science* **303**, 495-499.

Roberts, R. L., Barbieri, M. A., Pryse, K. M., Chua, M., Morisaki, J. H. and Stahl, P. D. (1999). Endosome fusion in living cells overexpressing GFP-rab5. *J. Cell Sci.* **112**, 3667-3675.

Roepstorff, K., Grandal, M. V., Henriksen, L., Knudsen, S. L., Lerdrup, M., Grovdal, L., Willumsen, B. M. and van Deurs, B. (2009). Differential effects of EGFR ligands on endocytic sorting of the receptor. *Traffic* **10**, 1115-1127.

Romagnoli, P., Layet, C., Yewdell, J., Bakke, O. and Germain, R. N. (1993). Relationship between invariant chain expression and major histocompatibility complex class II transport into early and late endocytic compartments. *J. Exp. Med.* **177**, 583-596.

Roux, A., Cappello, G., Cartaud, J., Prost, J., Goud, B. and Bassereau, P. (2002). A minimal system allowing tubulation with molecular motors pulling on giant liposomes. *Proc. Natl. Acad. Sci. USA* **99**, 5394-5539.

Schepis, A., Stauber, T. and Krijnse Locker, J. (2007). Kinesin-1 plays multiple roles during the vaccinia virus life cycle. *Cell Microbiol.* **9**, 1960-1973.

Simonsen, A., Lippe, R., Christoforidis, S., Gaullier, J. M., Brech, A., Callaghan, J., Toh, B. H., Murphy, C., Zerial, M. and Stenmark, H. (1998). EEA1 links PI(3)K function to Rab5 regulation of endosome fusion. *Nature* **394**, 494-498.

Stang, E. and Bakke, O. (1997). MHC class II-associated invariant chain-induced enlarged endosomal structures: a morphological study. *Exp. Cell Res.* **235**, 79-92.

Stenmark, H., Parton, R. G., Steele-Mortimer, O., Lutcke, A., Gruenberg, J. and Zerial, M. (1994). Inhibition of rab5 GTPase activity stimulates membrane fusion in endocytosis. *EMBO J.* **13**, 1287-1296.

Tanaka, Y., Kanai, Y., Okada, Y., Nonaka, S., Takeda, S., Harada, A. and Hirokawa, N. (1998). Targeted disruption of mouse conventional kinesin heavy chain, kif5B, results in abnormal perinuclear clustering of mitochondria. *Cell* **93**, 1147-1158.

Vale, R. D. and Hotani, H. (1988). Formation of membrane networks in vitro by kinesin-driven microtubule movement. *J. Cell Biol.* **107**, 2233-2241.

Verhey, K. J. and Hammond, J. W. (2009). Traffic control: regulation of kinesin motors. *Nat. Rev. Mol. Cell Biol.* **10**, 765-777.